Title

Release kinetics of metronidazole from 3D printed silicone scaffolds for sustained application to the female reproductive tract

Authors

Herold, Sydney E
Kyser, Anthony J
Orr, Margaret G
et al.

Publication Date

2023-06-01

DOI

10.1016/j.bea.2023.100078

Peer reviewed

Published in final edited form as:

Biomed Eng Adv. 2023 June ; 5: . doi:10.1016/j.bea.2023.100078.

Release Kinetics of Metronidazole from 3D Printed Silicone Scaffolds for Sustained Application to the Female Reproductive Tract

Sydney E. Herold[1,‡], **Anthony J. Kyser**[1,‡], **Margaret G. Orr**[2], **Mohamed Y. Mahmoud**[1,3], **Warren G. Lewis**[4,5], **Amanda L. Lewis**[4,5], **Jill M. Steinbach-Rankins**[1,6,7,*], **Hermann B. Frieboes**[1,6,8,9,*]

[1]Department of Bioengineering, University of Louisville, Louisville, KY, USA

[2]Department of Chemical Engineering, Bucknell University, Lewisburg, PA, USA

[3]Department of Toxicology and Forensic Medicine, Faculty of Veterinary Medicine, Cairo University, Egypt

[4]Department of Obstetrics, Gynecology and Reproductive Sciences, University of California San Diego, La Jolla, California USA

[5]Glycobiology Research and Training Center, University of California San Diego, La Jolla, California USA

[6]Department of Pharmacology and Toxicology, University of Louisville, Louisville, KY, USA

[7]Department of Microbiology and Immunology, University of Louisville, Louisville, KY, USA

[8]Center for Predictive Medicine, University of Louisville, Louisville, KY, USA

[9]UofL Health – Brown Cancer Center, University of Louisville, KY, USA

Abstract

Sustained vaginal administration of antibiotics or probiotics has been proposed to improve treatment efficacy for bacterial vaginosis. 3D printing has shown promise for development of systems for local agent delivery. In contrast to oral ingestion, agent release kinetics can be fine-tuned by the 3D printing of specialized scaffold designs tailored for particular treatments while enhancing dosage effectiveness via localized sustained release. It has been challenging to establish scaffold properties as a function of fabrication parameters to obtain sustained release. In particular, the relationships between scaffold curing conditions, compressive strength, and drug release kinetics remain poorly understood. This study evaluates 3D printed scaffold formulation and feasibility to sustain the release of metronidazole, a commonly used antibiotic for BV. Cylindrical silicone scaffolds were printed and cured using three different conditions relevant to potential future incorporation of temperature-sensitive labile biologics. Compressive strength and drug release were monitored for 14d in simulated vaginal fluid to assess long-term effects of

Correspondence: Hermann B. Frieboes, Department of Bioengineering, Lutz Hall 419, University of Louisville, KY 40292, USA. Tel.: 502-852-3302; Fax: 502-852-6806; hbfrie01@louisville.edu.

‡These authors contributed equally

*Joint senior authorship

fabrication conditions on mechanical integrity and release kinetics. Scaffolds were mechanically evaluated to determine compressive and tensile strength, and elastic modulus. Release profiles were fitted to previous kinetic models to differentiate potential release mechanisms. The Higuchi, Korsmeyer-Peppas, and Peppas-Sahlin models best described the release, indicating similarity to release from insoluble or polymeric matrices. This study shows the feasibility of 3D printed silicone scaffolds to provide sustained metronidazole release over 14d, with compressive strength and drug release kinetics tuned by the fabrication parameters.

Keywords

Metronidazole; 3D printed scaffolds; silicone scaffolds; drug release kinetics; bacterial vaginosis

Introduction

Bacterial vaginosis (BV) is a common vaginal condition diagnosed in approximately 1 in 3 women of reproductive age in the U.S. [1]. BV is characterized by low levels of healthy, lactic acid producing, lactobacilli and overgrowth of facultative and anaerobic bacteria in the vagina [1–3]. One of the prominent bacterial taxa associated with BV is *Gardnerella vaginalis*, which is susceptible to weak acid stress in the normally low pH of the healthy female genital tract (pH 4.5) [3–5]. Symptoms of BV may include an abnormally thin malodorous discharge and vaginal irritation [2, 6], although some women do not report symptoms. BV has been associated with higher risks of many adverse health outcomes, including pregnancy complications such as preterm delivery, and increased risk of acquiring HIV and other sexually transmitted infections (STIs) [1].

The current standard of treatment for women diagnosed with BV is a 5–7 day oral or topical regimen with an antibiotic such as metronidazole, with twice daily oral regimens or once-daily intravaginal gel application [7, 8]. Topical administration avoids the adverse effects of oral metronidazole administration while allowing localized drug release. In fact, a variety of dosage forms have been developed for vaginal administration of antibiotics and other active agents, including vaginal gels, suppositories, nanoparticle-based systems, and intravaginal rings (IVRs) [9–15]. Yet, with the exception of IVRs, these dosage forms act transiently and necessitate frequent daily administrations to exert therapeutic effect. Furthermore, the leakage and associated messiness of current dosage forms can result in a lack of user adherence to prescribed administration schedules, which can, in turn reduce effectiveness and promote antibiotic-resistance. As an alternative strategy, probiotic *Lactobacillus* have demonstrated some success in restoring healthy attributes to the vaginal environment [16]. However, much like antibiotic dosage forms, there are a dearth of topical probiotic or combination dosage forms that provide sustained or phased co-delivery of one or more active antimicrobial agents.

One of the few dosage forms that has demonstrated success in attaining long-term intravaginal delivery are IVRs. A variety of polymers including silicone, polyurethanes, and ethylene vinyl acetate (EVAc) have been used to facilitate the release of hydrophobic molecules, such as hormones, and more recently antibiotics, such as metronidazole, for

intravaginal applications [17, 18]. Silicone, in particular, has been shown to have exceptional biocompatibility, low surface tension for uniform drug distribution, as well as biodurability in low pH environments [19]. However, IVR fabrication typically relies on molding techniques that can be susceptible to deformation and contamination, in addition to harsh solvents, temperatures, and multistep fabrications that may be less amenable to the inclusion of more labile biologic agents [20].

A proposed solution to improve upon the duration of administration, multi-therapeutic compatibility of manufacturing, and throughput of the fabrication process, is to utilize extrusion-based 3D printing. This type of printing, in combination with computer aided design (CAD), can be used to fabricate architectures with discrete compartments to facilitate the release of different active agents from sequentially-printed layers [21]. These features enable the fabrication of simple as well as complex architectures that provide sustained release and increased bioavailability of drug at a localized site [22, 23]. While 3D printing has been utilized for a few vaginal applications [24–29], it has not been extensively studied for intravaginal drug delivery. One exception are progesterone-loaded 3D printed vaginal rings, which have shown promise in producing consistent complex geometric designs [24].

In pharmaceutics, the use of silicone as an ink for 3D printing has been both advantageous and complex [30–32]. As with IVRs and vaginal pessaries, 3D printing inks can be customized for drug loading, using modified concentrations and favorable architectures for sustained release[33–39]. Furthermore, incorporation of crosslinkers and co-polymers into the ink can alter release profiles and mechanical integrity of 3D printed structures[40]. Modifications to concentration and ink formulation can change ink viscosity, leading to alterations in the resolution of 3D extrusion printed architectures [41, 42]. In addition to formulation challenges, translation to commercialized products produced with individualized pharmaceutical applications remains an elusive goal [43].

Design optimization can require numerous experimental iterations depending on the critical parameters of interest [44]. Complementing formulation development with mathematical modeling enables the knowledge of physical parameters, such as drug diffusion coefficients and polymer relaxation coefficients, to be combined with mathematical equations representing a given system, to help establish, predict, and validate parameters integral to achieving design criteria [45]. In particular, mathematical modeling may be useful in establishing key outcomes, such as release kinetics, mechanical integrity, and degradation as a function of the post-processing conditions of new 3D printed dosage forms [46–48].

In this study, one of the key considerations for 3D printed scaffold design was the ability to prolong metronidazole release for durations of one week or longer. Additionally, since future scaffolds could be designed to co-deliver other active agents, including more labile biologics, the duration and temperature of post-print processing were primary parameters of interest. In order to help elucidate the relationships between scaffold curing conditions, compressive strength, and drug release kinetics, this study evaluated the effects of scaffold curing time and temperature on the metronidazole release. Three different 3D printed silicone scaffold formulations were fabricated, which varied in their post-print curing conditions, and evaluated for *in vitro* drug release in simulated vaginal fluid (SVF). The

post-print curing conditions were considered contingent on applications towards biological stress responses [49–53]. Additionally, differences in tactile properties were considered to provide comfortable application and residence [54, 55]. Scaffolds were axially and radially compressed to determine compressive strength as a function of curing conditions. In parallel, we utilized mathematical modeling to evaluate the impact of post-print curing on antibiotic release kinetics. Potential mechanisms of drug release were assessed via established kinetic models, including zero order, first order, Higuchi, Korsmeyer-Peppas, Hixson-Crowell, and Peppas-Sahlin [56]. The modeling was employed to give insight into the diffusion-controlled release of metronidazole from the formulated scaffolds, in order to evaluate sustained drug delivery.

Materials and Methods

Materials

The ink base polymer consisting of a mixture of vinyl-terminated polydimethylsiloxane (70%) and vinyl, methyl-modified silica (30%), and the crosslinking agent, methylhydrosiloxane-dimethylsiloxane copolymer, trimethylsiloxane-terminated, were purchased from Allevi, Inc. (Philadelphia, PA). Dimethyl sulfoxide (DMSO, Fischer Scientific, B231-1), and Metronidazole (Sigma Aldrich, M3761-5G) were used to formulate the ink for 3D printing. Simulated vaginal fluid (SVF) was prepared as in [57, 58].

3D Printed Silicone Scaffold Synthesis

Printable Silicone Ink—Briefly, metronidazole (55 mg) was weighed, ground to a fine powder with a mortar and pestle, and added to a microcentrifuge tube containing 60 μL DMSO. The ink consisting of 1.0 g:0.1 g of the base polymer and crosslinking agent, was added and vortexed to ensure homogeneity. The ink was vigorously mixed with a spatula for a minimum of 5 min. The base and crosslinker undergo an exothermic hydrosilylation reaction when exposed to higher temperatures and becomes vulcanized without producing any by-products [59–61]. The base polymer is crosslinked through the transfer of hydrogen atoms and conversion to carbon sp^3 hybridization [61].

Scaffold Printing—A 1 mL aliquot of metronidazole-containing ink was loaded into a 5 mL syringe and placed into the CORE head of the Allevi 3 Bioprinter. A customized STereoLithography (STL) file was created in the form of a cylindrical capsule. The capsule dimensions were sized for a mouse model of BV: 5 mm in height, 4 mm in diameter, with a shell thickness of 0.5 mm. In comparison of CAD drawings of ring and cylindrical capsule designs, with well-defined architecture, the cylindrical capsule with filleted edges – a commonly utilized design in vaginal applicators [62] – had surface area >4 times the ring's surface area, indicating its suitability for more favorable drug release than a ring geometry.

The Allevi 3 Bioprinter was used to 3D print all scaffolds. The extrusion pressure was set at 100 psi, the CORE head of the extruder was set at 30°C, and the extrusion flow rate was set at 5 mm/sec The layer height for printing was set at 0.2 mm, the infill distance was fixed at 0.35 mm with zig-zag infill type, and a 23G needle gauge was used for extruding the

formulated bioink. Scaffolds were printed in a petri dish using the STL file as a printing template and were then subjected to one of three different post-print curing conditions.

Curing and Storage Time/Conditions—Three different 3D printed silicone scaffold formulations were fabricated, with variations in their post-print curing conditions chosen as representatives for sustained release evaluation, biological stress response and tactile properties. Scaffold A was cured at 50°C for 4 hr, followed by incubation at 4°C for 72 hr. This condition considers the potential of future biologic inclusion by minimizing high temperature exposure which can lead to biologic inactivation [63, 64]. *Lactobacillus* strains have shown thermophilic tendencies and produce bacteriocins with thermostability at higher temperatures [65–67]. Scaffold B was cured at 50°C for 4 hr, followed by incubation at 20°C for 24 hr, which sought to improve mechanical integrity while minimizing exposure to temperatures >50°C. Scaffold C was cured at 50°C for 24 hr to evaluate prioritization of mechanical integrity over biologic inactivation. Metronidazole retains thermostability at 50°C and has been utilized in hot melt extrusion techniques at higher temperatures [68–71]. Selected scaffold curations were contingent on preliminary mechanical integrity evaluations of a range of curing parameters with the consideration of biological inclusion.

Metronidazole Incorporation—Metronidazole concentration of 50 μg/mg was selected for initial loading, as it was found to eliminate anaerobes including, *Gardnerella, Prevotella,* and *Bacteroides* species based upon MIC_{50} values (<8 μg/mL) [72] and the susceptibility breakpoint concentration for metronidazole defined by Clinical and Laboratory Standards Institute (CLSI). In comparison, commensal lactobacilli have metronidazole MIC_{50} >128 μg/ml [72]. The theoretical scaffold loading was calculated based on scaffold weight and metronidazole concentration in the silicone ink (Eq. 1).

$$Theoretical\ Loading\ (\mu g) = Scaffold\ Mass\ (mg) * Drug\ Concentration\ (\mu g/mg) \quad \text{(Eq. 1)}$$

Biocompatibility Testing

Biocompatibility of the 3D printed scaffolds was evaluated in the presence of vaginal epithelial cells. MTT assay was used to determine *in vitro* safety of blank and metronidazole-containing silicone scaffolds, in a VK2/E6E7 cell line. Cells were plated at a density of 300,000/well in a 12-well plate and incubated for 24 hr at 37°C. Media only (untreated cells) and 10% DMSO were used as viable and non-viable cell controls. After 24 and 72 hr incubation, 100 μL of MTT labeling reagent was added to each well and incubated at 37°C for 4 hr, followed by adding 1 mL of lysis buffer containing 10% sodium dodecyl sulfate and 0.01 M hydrochloric acid. After 16 hr incubation, the absorbance was read at 570 nm (SYNERGY Microplate Reader, Biotek Instruments Inc) and normalized to cell-only absorbance to attain the relative percent of cell viability.

Mechanical Testing

Compression Testing—Compressive strength of the scaffolds was evaluated as a function of curing condition. Blank silicone and metronidazole-containing silicone scaffolds

were assessed after curing with the following conditions: 50°C for 4 hr, followed by incubation at 4°C for 72 hr; 50°C for 4 hr, followed by incubation at 20°C for 24 hr; and 50°C for 24 hr (Scaffold A, B, and C, respectively). Scaffolds were assessed immediately post-cure, and after 24 hr or 14 d in SVF.

Compression in the axial and radial directions was measured using Instron 5569 testing system, and data were extrapolated using Instron Bluehill software (Norwood, MA). Compression test parameters were selected to represent range with which commercial IVRs have been tested [73, 74]. A 5 kN load cell was used, and applied force was varied between 0.6 and 1.6 N. Transducer was lowered to scaffold surface prior to the test and transducer displacement was set to 1 mm with displacement rate of 1 mm/min. These configurations are equivalent to 20% or 25% compression in axial and radial directions, respectively.

Tensile Testing—Scaffold tensile strength, strain, and elastic modulus were evaluated as function of curing condition. Blank and metronidazole-containing silicone inks were used to 3D-print die cut C dog bone specimens scaled in accordance to ASTM D412 standards and evaluated after curing under the three conditions chosen for this study. Tensile strength was measured using MTI-2K-mini testing system, and data were extrapolated with MTI Universal Testing Systems software (Houma, LA). Initial gauge length was measured with calipers, marked prior to elongation, and re-measured after rupture to determine strain. A 50 kN load cell was used to perform tensile testing with velocity at 500 mm/min until fracture. Dog bone specimens were preloaded prior elongation.

Evaluation of Drug Release

In vitro drug release was evaluated in SVF. Metronidazole-containing silicone scaffolds were submerged in 1 mL SVF (pH 4.2) and incubated at 37°C to mimic physiological temperature. Metronidazole release was evaluated at 2, 4, 8 hr, and after 1, 2, 3, 4, 5, 6, 7, 8, 9, 10, and 14 d. At established times, SVF was removed from 1.5 mL tubes, scaffolds were washed with 4x PBS, and fresh SVF was added. Amount of metronidazole in each eluate sample was determined by reading absorbance (320 nm, Gen 5 app, BioTek Synergy H1 Microplate Reader) and correlating with metronidazole standard curve. Cumulative metronidazole release was calculated as μg of metronidazole released per mg scaffold and as % total loaded, as in Eq. 2.

$$\%\ Cumulative\ Drug\ Release = \frac{[Drug]_t}{[Drug]_{total}} * 100 \quad \text{(Eq. 2)}$$

where $[Drug]_t$ refers to amount released at time t and $[Drug]_{total}$ refers to total loaded.

Mechanism of Drug Release

To assess the mechanism of drug release, representative kinetic models were used to analyze the drug release data. The zero order kinetic model describes drug release independent of drug concentration in solution (Eq. 3) [75],

$$Q_t = Q_0 + kt \quad \text{(Eq. 3)}$$

where Q_t is drug amount dissolved in time t, Q_0 is initial drug amount in solution, and k is zero order rate constant. The first order kinetic model describes drug release dependent on drug concentration (Eq. 4)[75],

$$logC = logC_0 - \frac{kt}{2.303} \quad \text{(Eq. 4)}$$

where C is drug concentration at time t, C_0 is initial drug concentration, and k is first order rate constant. The simplified Higuchi model describes drug release from polymeric systems, where dissolution is the main method of drug transfer (Eq. 5) [76].

$$\frac{M_t}{M_\infty} = k\sqrt{t} \quad \text{(Eq. 5)}$$

where M_t/M_∞ is cumulative drug amount released at time t, and k is Higuchi rate constant, also known as the diffusion coefficient. The Korsmeyer-Peppas model describes drug release from polymeric matrices (Eq. 6) [75].

$$\frac{M_t}{M_\infty} = k't^n \quad \text{(Eq. 6)}$$

where M_t/M_∞ is cumulative drug release at time t, k' is drug release coefficient, and n describes a mechanism of diffusion. The Hixson Crowell cube root model utilizes the proportionality of a particle's area to its volume to describe drug release (Eq. 7) [77],

$$W_0^{1/3} - W_t^{1/3} = kt \quad \text{(Eq. 7)}$$

where W_0 is the initial amount of drug, W_t is the remaining amount of drug at time t, and k is the rate constant. The Peppas-Sahlin model accounts for effects of Fickian diffusion and polymer chain relaxation during drug release (Eq. 8) [78],

$$\frac{M_t}{M_\infty} = k_d t^m + k_r t^{2m} \quad \text{(Eq. 8)}$$

where M_t/M_∞ is cumulative drug release at time t, k_d is kinetic constant associated with Fickian diffusion, k_r is kinetic constant associated with polymer chain relaxation, and m is the purely Fickian diffusion exponent [78].

Each model's adequacy was evaluated using MATLAB Curve Fitting Toolbox. Once the parameters were obtained, graphs were constructed using Microsoft Excel. All models were obtained by plotting cumulative percent drug release against time and using the Custom Equation option to fit the model to the data.

Statistics

Compression measurements and drug release were performed with a minimum n=3 replicates. Error bars denote standard deviation (SD) and results are reported as mean ± SD. Minitab was used to statistically analyze drug release. A Grubbs' test was utilized to determine the presence of outliers ($p \leq 0.05$) to be removed. One-way ANOVA was used to

evaluate statistically significant differences in metronidazole release values and compression testing results between scaffold designs. Paired t-test was used to evaluate tensile testing results to determine statistical significance between blank and metronidazole-containing scaffolds.

Results

The 3D-printed scaffold design in this study is shown schematically in Figure 1A and as an actual image in Figure 1B.

Biocompatibility: Cell Viability

Preliminary evaluation of the 3D printed scaffolds in the presence of VK2 cells showed no statistically significant decrease in cell viability for both blank and metronidazole-containing scaffolds relative to untreated cells (Figure 1C). In contrast, 10% DMSO- treated cells showed significant ($p \leq 0.0001$) decrease in cell viability relative to scaffold-treated and untreated cells.

Mechanical Properties: Compression

The load required to compress each scaffold was evaluated as a function of scaffold curing conditions immediately post-cure, and after 24 hr and 14 d in SVF. All scaffolds were compressed by 20% of height and 25% of diameter, in axial and radial directions, respectively.

Axial Compression—The load required to axially compress blank scaffolds immediately post-cure and after 24 hr in SVF was lower after curing for 4 hr at 50°C (Scaffolds A and B) compared to scaffolds cured for 24 hr at 50°C (Scaffold C) (Figure 2A and Figure 2B). Similar trends were observed for metronidazole-containing scaffolds post-cure (Figure 2D) but not after 24 h in SVF, in which case the load to compress Scaffold C was as low as for the other formulations (Figure 2E). For Scaffolds A and B, the load required to achieve axial compression was similar between post-**c**ure and 24 hr cure groups. However, a higher load was required for compression for these two formulations after 14 d in SVF but not for Scaffold C (Figure 2C and Figure 2F). Overall, and based on the average of all immersion conditions for each scaffold type, the load required to axially compress blank scaffolds was approximately 8-fold, 12-fold, and 18-fold higher for Scaffolds A, B, and C, respectively, than that needed for similar compression of metronidazole-containing scaffolds. These results indicate that drug incorporation at the specified concentration may weaken the scaffolds under axial compression.

Radial Compression—Radial compression was measured to account for additional forces the scaffolds may experience in the vaginal environment. The trends observed with axial compression as a function of curing conditions were also evident with radial compression, except that the loads required for radial compression were generally lower than for axial compression. The load required to radially compress blank scaffolds was approximately 21-fold, 25-fold, and 30-fold (for Scaffolds A, B, and C) higher than that needed for similar compression of metronidazole-containing scaffolds. As with

axial compression, these results suggest that metronidazole incorporation may weaken the scaffolds under radial compression. Lastly, both blank and metronidazole-containing silicone scaffolds exhibited lower compressive strength in the radial direction, relative to the axial direction.

Mechanical Properties: Strain, Tensile Strength, and Elastic Modulus

Mechanical properties through tensile testing were measured as a function of curing conditions (Scaffold A, B, or C) immediately post-cure utilizing 3D-printed dog bone specimens. In both blank and metronidazole-containing scaffold groups, scaffolds cured for 24 hr at 50°C (Scaffold C) exhibited the highest strain (Figure 4A). Compared to blank scaffolds, metronidazole-containing versions exhibited 4-fold lower strain for Scaffolds A and B and 2-fold lower for Scaffold C. Tensile strength and elastic modulus of Scaffold C were highest compared to Scaffolds B and C (Figure 4B and Figure 4C). Strength was higher for blank Scaffolds B and C compared to their metronidazole-containing versions, while elastic modulus was higher for blank Scaffold C compared to the metronidazole-containing version (Figure 4C).

Drug Release

The cumulative release of metronidazole from the 3D printed silicon scaffolds is shown as a function of percent of total loading for 24 h (Figure 5A) and 14 d (Figure 5B), while amount released was >55 μg/ 1 ml SVF from 1 to 14 d (Figure 5C). Overall, the scaffolds showed a steady release within the first 6 hr, following a common trend observed with small molecules [7, 56, 79, 80]. Post-print curing condition proved to have an effect on cumulative release. Scaffold A showed the highest metronidazole release, with 15.8±2.4% release occurring in the first 24 hr, followed by a steady increase to 54.1±2.9% after 14 d. Scaffold B showed intermediate levels of release, with 10.2±0.8% of drug released during the first 24 hr and 40.8±4.1% after 14 d. Scaffold C showed the least overall release with 8.7±2.4% release over the first 24 hr and only 33.7±5.1% release after 14 d. For short-term (24 hr) and long-term (14 d) drug release, statistical significance was observed between Scaffolds A and B and between Scaffolds A and C ($p \leq 0.05$), but not between Scaffolds B and C. Post-print curing condition of Scaffold A (4 hr at 50°C followed by 72 hr at 4°C) provided sufficient mechanical integrity to extend drug release over 14 d. Accordingly, this formulation may be suitable for eventual inclusion of more labile biologics.

Kinetic Models of Drug Release

Previously developed mathematical kinetic models are useful to evaluate potential mechanisms of drug release, and were applied here to study metronidazole release from the 3D printed silicone scaffolds. For each scaffold formulation, *in vitro* release curves (Figure 5) were fitted to various representative kinetic models to describe potential mechanisms of release (Figures 6–8). The resulting correlation values and rate constants for all models are summarized in Table 1.

Each model exhibited similar R^2 values across the three different post-print curing conditions; therefore, the most appropriate condition can be selected without it affecting

the mechanism of metronidazole release. The Higuchi, Korsmeyer-Peppas, and Peppas-Sahlin models best described the release of metronidazole from the 3D printed silicone scaffolds. The Higuchi model had an $R^2 = 0.9918$ (Scaffold A), $R^2 = 0.9955$ (Scaffold B), and $R^2 = 0.9954$ (Scaffold C). The Korsmeyer-Peppas model had an $R^2 = 0.9931$ (Scaffold A), $R^2 = 0.9959$ (Scaffold B), and $R^2 = 0.9958$ (Scaffold C). Lastly, the Peppas-Sahlin model had an $R^2 = 0.9990$ (Scaffold A), $R^2 = 0.9990$ (Scaffold B), and $R^2 = 0.9980$ (Scaffold C). These three models outperformed even when considering $R^2_{adjusted}$ (as defined in [77]) that takes into account the higher number of parameters in the Korsmeyer-Peppas and Peppas-Sahlin models.

These results indicate that the release of metronidazole, a hydrophobic drug, from silicone, a hydrophobic polymer, is similar to drug release from an insoluble matrix or from a polymeric matrix [7, 80]. The zero order model showed the lowest correlation to experimental metronidazole release with an $R^2 = 0.6862$ (Scaffold A), $R^2 = 0.7667$ (Scaffold B), and $R^2 = 0.7699$ (Scaffold C), indicating the release of metronidazole from 3D printed silicone scaffolds is not independent of drug concentration in solution [75, 81]. This is confirmed by the first order model showing significantly improved correlation compared to the zero order model for all post-print curing conditions, although not quite reaching the performance of the best three models.

Discussion

Metronidazole-containing 3D printed silicone scaffolds were fabricated to evaluate sustained release kinetics with the ultimate goal of developing new treatment modalities for BV. Metronidazole, a model hydrophobic active agent and commonly used drug for BV treatment, was incorporated into silicone by dissolving in DMSO and physically mixing [82]. Three representative post-print curing conditions were evaluated to enhance mechanical integrity prior to immersing each scaffold in SVF for drug release studies and fitting of release profiles to common kinetic models. The biocompatibility of the formulated blank and metronidazole-containing scaffolds was evaluated with vaginal epithelial cells *in vitro*, providing a preliminary safety assessment. To better understand the relationship between curing condition and cumulative metronidazole release, the compressive strength of metronidazole-containing scaffolds was evaluated immediately post-cure and following immersion in SVF for 24 hr and 14 d, to measure changes in mechanical integrity as could occur in the vaginal environment.

Figure 2 and Figure 3 indicate that a short curing duration of 4 hr (Scaffolds A and B) may leave scaffolds more mechanically susceptible in the short term to compression (e.g., potentially less dense or more porous) than scaffolds cured for 24 hr (Scaffold C). On the other hand, the shorter cure duration followed by refrigerated incubation of Scaffold A (Figure 5) enabled more rapid metronidazole release. This scaffold showed the greatest cumulative drug release over 14 d (Figure 5) while by that time having the largest axial and radial compressive strengths relative to Scaffolds B and C (Figures 2F and Figure 3F). Interestingly, Scaffold A became more mechanically stable by 14 d than Scaffold B (incubated post-cure at room temperature) (Figure 2F and Figure 3F).During this prolonged

immersion in SVF, the higher amount of metronidazole released from Scaffold A (Figure 5B) would increase the surface area of the scaffold via porosity, enabling greater molecular interaction between the base polymer and functional ionic salts found in SVF to further mechanically strengthen the construct [83]. Further, a shorter exposure to high temperature during curing would entail a lower degree of polymer crosslinking, leaving a higher amount of additives that promote crystallization, which has been shown to have a competing effect with crosslinking in regards to mechanical strength [84].

Another and potentially more significant observation was the decrease in compressive and tensile strength with the inclusion of metronidazole into the scaffold formulations. The load required to compress blank scaffolds was several fold higher than that needed for similar compression of metronidazole-containing scaffolds (Figures 2 and 3). Stress required to rupture blank Scaffold B and Scaffold C was similarly several fold higher (Figure 4), while that for metronidazole versions was comparable among the scaffold formulations. These results suggest that metronidazole (at the concentration used in this study) may somewhat weaken the scaffold structure or affect the effectiveness of crosslinking mechanism post-print. Thus, one could argue that drug incorporation into the ink formulation was achieved by retaining homogeneity and high printing resolution at the expense of mechanical strength. A lower cross-linking density of methylhydrosiloxane-dimethylsiloxane copolymer, trimethylsiloxane-terminated, due to the addition of a therapeutically relevant drug dose, consequently contributed to the decrease in scaffold strength, consistent with previous silicone curing studies [84–87].

Primary concern of mechanical strength of the scaffolds was based on the scaffold's ability to retain the designed architecture for tailored release, for which the scaffolds demonstrated their elasticity when compressed axially at 20% (1 mm) of scaffold height and radially 25% (1 mm) of scaffold diameter. A past study identified the biomechanics of the vaginal supportive tissue complex of rodents to be highly dynamic [88], indicating the need for scaffold versatility with elasticity in both the axial and radial compression. Furthermore, anisotropy analysis on murine vaginal walls has shown a higher linear modulus in the circumferential direction [89], underscoring the need for compression resistance of the scaffolds radially. A previous analysis of biaxial strength of smooth muscle from vaginal walls extracted from mice showed a change in axial forces of 10–18 mN with contractions induced by physiological *in vivo* pressures [90]. In this study, metronidazole-containing scaffolds were able to withstand axial compression an order of magnitude higher than these values (Figure 2). In humans, during voluntary pelvic floor muscles contraction, peak isometric forces of 0.1 and 0.06 N were measured from the anterior and posterior vaginal walls, respectively, with displacement ranges of 0.6–0.8 mm [91], These values are comparable to the circumferential forces withstood by the metronidazole-containing scaffolds (Figure 3).

Previous evaluation of mechanical strength in IVRs has measured compression strength in EVA-R intravaginal [73] and TFV-HPEU 20 [74] rings, which have compressive loads between 1 and 1.25 N when compressed by 20% of their original outer diameter [73]. Similarly, uniaxial mechanical testing of TFV-HPEU IVRs resulted in a required compressive load less than 1 N to compress rings by 1 mm [74]. In this study,

characterization of material properties of ink cured at different conditions was assessed independently of the scaffold's cylindrical geometry through tensile testing. The results indicate a propensity for higher resistance for inks cured for a longer period at higher temperatures, regardless of scaffold architecture. Furthermore, the measured scaffold tensile and compressive strengths highlight the potential for self-application and removal without rupture or deformation [92]. Thus, the mechanical strength of the 3D-printed scaffolds in this study suggests that they may be effective for drug release while retaining suitable mechanical properties to be inserted and applied for intravaginal anti-infection applications [73, 93, 94].

The use of silicone as a means of drug delivery has been previously studied and modeled. Ibuprofen and diclofenac have been incorporated into a multi-layered silicone matrix system and the release kinetics were modeled using a numerical model [95]. Model parameters included diffusion, effective dissolution rate, and solubility coefficients. Based on experimental data, the fabricated numerical model could be used to design controlled drug release multi-layer silicone devices. In another study, dexamethasone was incorporated into silicone and the release was fitted to a previously derived equation [96]. The model highlighted the impact that system geometry, size, and composition may have on the drug release kinetics.

The release kinetics of metronidazole has been previously studied using a wide variety of computational models, materials, and dosage forms. In one study, metronidazole was incorporated into HPMC, psyllium, and Carbopol to fabricate a floating dosage form to treat peptic ulcer disease [56]. Metronidazole release was modeled using similar models to this study, including zero-order kinetic, first-order kinetic, Higuchi, Hixson-Crowell, Power law, and the Weibull model. Metronidazole release from tablets was best modeled by the power law, as the release is dependent on Fickian diffusion and polymer relaxation. In another study, metronidazole was incorporated into mesostructured silica-based materials to treat bone disease [7]. Metronidazole release was found to differ based on the addition of various types of organic groups onto the silica. Drug release was adequately modeled by the Korsmeyer-Peppas model, which indicated diffusion-controlled release. Metronidazole has also been incorporated into alginate beads with calcium silicate acting as a porous carrier to facilitate release [97]. Metronidazole release using similar models in this study was modeled in [97], additionally including linear probability, log probability, and reciprocal powered time models. Release was shown to be best modeled by reciprocal powered time, Weibull, and log probability models.

In this study, while post-print curing condition did not show an effect on the mechanism of metronidazole release from silicone (Table 1), it proved to have an effect on cumulative release. Due to hydrophobicity of metronidazole, no scaffold exhibited substantial burst release within the first 24 hr (Figure 5), in agreement with release profiles observed for metronidazole from other delivery platforms [11, 56]. In congruence with *in vitro* data, metronidazole release from Scaffolds A, B, and C was best modeled by the Higuchi, Korsmeyer-Peppas, and Peppas-Sahlin kinetic models. All three models have previously been used to adequately describe drug release from polymeric matrices, suggesting that drug release from 3D printed silicone scaffolds can be modeled similarly to release from

polymeric matrix systems. The Higuchi model describes drug release from matrix systems via diffusion-controlled release and relies on the following assumptions: (*i*) initial drug concentration is much higher than solubility drug concentration, (*ii*) drug diffusion takes place in one dimension (edge effects are negligible), (*iii*) drug particles are much smaller than the delivery system, (*iv*) drug diffusivity is constant, and (*v*) perfect sink conditions exist in the release environment [75].

In contrast, the Korsmeyer-Peppas model is a semi-empirical model that utilizes the first 60% of the drug release curve to determine the mechanism of drug release using the value of the release exponent, n [75]. For all scaffolds, $0.45<n<0.89$ indicated anomalous transport (assuming cylindrical geometry), suggesting that the mechanism of drug release is a combination of Fickian diffusion and polymer relaxation. The release data was further fit to the Peppas-Sahlin model [78], which uses two terms to isolate the drug transport attributed to either Fickian diffusion or polymer relaxation. For all scaffolds, k_d was much greater than k_r (Table 1), indicating that the mechanism of metronidazole release from the silicone scaffolds is mainly Fickian diffusion. Additionally, all scaffolds exhibited negative k_r, indicating that polymer chain relaxation may be insignificant in metronidazole release from silicone [98]. For comparison, we also evaluated the Weibull model as an additional candidate to describe metronidazole release from 3D printed scaffolds. Drug release from all three scaffolds was adequately modeled by the Weibull model with $R^2 > 0.98$. This model is a general empirical equation that has been widely applied to drug release across dosage forms. However, it is limited in its ability to provide comparisons between *in vivo* and *in vitro* release and lacks many parameters that can be related to dissolution rate [77].

The metronidazole release of the scaffolds evaluated in this study is considered sufficient for therapeutic effect against *Gardnerella vaginalis*, being >55 μg/ 1 ml SVF from 1 to 14 d for each scaffold (Figure 5C). Previous work has identified the minimum inhibitory concentration and bactericidal concentration of metronidazole to be 16 μg/ml and 32 μg/ml, respectively, against *Gardnerella vaginalis* biofilm viability at concentration of 10^8 CFU/ml [99]. Further, the drug release profiles of the scaffolds in this study followed trends similar to those of metronidazole-loaded mucoadhesive microspheres with antibacterial activity for vaginal administration [100].

Towards the goal of joint probiotic and antibiotic delivery, the scaffolds did undergo pH testing in SVF to confirm that pH remained stable (4.5) (data not shown), as could occur with Scaffolds A and B due to potential release of byproducts such as acetic acid due to shorter periods of crosslinking [101]. The dimensions of the evaluated scaffolds correspond with an appropriate size for testing in an experimental mouse model, and the wall thickness and infill distance were chosen to provide optimum resolution of diameter and height with the intention of future inclusion of probiotic bacteria in the scaffold core. With further development, the proposed core-shell scaffold could be designed to release beneficial bacteria immediately following release of metronidazole from the outer shell. Next steps include developing printable formulations that incorporate live bacteria and evaluating the associated release mechanisms. This study, focusing on the potential effect of fabrication parameters on sustained antibiotic release, represents a key step towards this goal.

Conclusion

With increasing drug-resistant cases of sexually transmitted diseases, alternative treatments via intravaginal delivery to provide localized application and improve bioavailability have been developed[102, 103]. High rates of recurrent BV further highlight the critical need for new treatment modalities [104]. Solutions using 3D-printing and other platforms for localized intravaginal delivery may address this crucial need. Through the modeling of release kinetics from 3D printed scaffolds loaded with the commonly used drug metronidazole, this study provides insight into the capability for sustained release from a biocompatible material. Longer term, we propose that a platform that can sustain the delivery of both antibiotics and live probiotic bacteria may enable a new approach for vaginal delivery of therapeutics.

Acknowledgments and Disclosures

The authors declare no competing financial interest.

Funding

This work was supported in part by National Institutes of Health / National Institute of Allergy and Infectious Diseases grants R01AI168475 and 5R01AI139671 (Frieboes & Lewis).

Abbreviations

3D	3-Dimensional
BV	Bacterial vaginosis
CAD	Computer-aided design
EVAc	Ethylene-vinyl acetate copolymer
FTR	Female reproductive tract
HIV	Human immunodeficiency virus
IVR	Intra-vaginal ring
MET	Metronidazole
STI	Sexually transmitted disease
SVF	Simulated vaginal fluid

References

[1]. Bradshaw CS, Morton AN, Hocking J, Garland SM, Morris MB, Moss LM, Horvath LB, Kuzevska I, Fairley CK, High recurrence rates of bacterial vaginosis over the course of 12 months after oral metronidazole therapy and factors associated with recurrence, J Infect Dis, 193 (2006) 1478–1486. [PubMed: 16652274]

[2]. Ravel J, Moreno I, Simón C, Bacterial vaginosis and its association with infertility, endometritis, and pelvic inflammatory disease, Am J Obstet Gynecol, 224 (2021) 251–257. [PubMed: 33091407]

[3]. Fredricks DN, Fiedler TL, Marrazzo JM, Molecular identification of bacteria associated with bacterial vaginosis, N Engl J Med, 353 (2005) 1899–1911. [PubMed: 16267321]

[4]. Sheiness D, Dix K, Watanabe S, Hillier SL, High levels of Gardnerella vaginalis detected with an oligonucleotide probe combined with elevated pH as a diagnostic indicator of bacterial vaginosis, J Clin Microbiol, 30 (1992) 642–648. [PubMed: 1372621]

[5]. O'Hanlon DE, Moench TR, Cone RA, In vaginal fluid, bacteria associated with bacterial vaginosis can be suppressed with lactic acid but not hydrogen peroxide, BMC Infect Dis, 11 (2011) 200. [PubMed: 21771337]

[6]. Spiegel CA, Bacterial vaginosis, Clin Microbiol Rev, 4 (1991) 485–502. [PubMed: 1747864]

[7]. Czarnobaj K, Sawicki W, The sol-gel prepared SiO2-CaO-P2O5 composites doped with Metronidazole for application in local delivery systems, Pharm Dev Technol, 17 (2012) 697–704. [PubMed: 21480825]

[8]. Paavonen JA, Brunham RC, Vaginitis in Nonpregnant Patients: ACOG Practice Bulletin Number 215, Obstetrics & Gynecology, 135 (2020) 1229–1230.

[9]. Sharifzadeh G, Hezaveh H, Muhamad II, Hashim S, Khairuddin N, Montmorillonite-based polyacrylamide hydrogel rings for controlled vaginal drug delivery, Mater Sci Eng C Mater Biol Appl, 110 (2020) 110609. [PubMed: 32204060]

[10]. Verstraete G, Vandenbussche L, Kasmi S, Nuhn L, Brouckaert D, Van Renterghem J, Grymonpré W, Vanhoorne V, Coenye T, De Geest BG, De Beer T, Remon JP, Vervaet C, Thermoplastic polyurethane-based intravaginal rings for prophylaxis and treatment of (recurrent) bacterial vaginosis, Int J Pharm, 529 (2017) 218–226. [PubMed: 28663088]

[11]. Pathak M, Turner M, Palmer C, Coombes AG, Evaluation of polycaprolactone matrices for the intravaginal delivery of metronidazole in the treatment of bacterial vaginosis, J Biomater Appl, 29 (2014) 354–363. [PubMed: 24682036]

[12]. Verstraelen H, Vervaet C, Remon JP, Rationale and Safety Assessment of a Novel Intravaginal Drug-Delivery System with Sustained DL-Lactic Acid Release, Intended for Long-Term Protection of the Vaginal Microbiome, PLoS One, 11 (2016) e0153441. [PubMed: 27093291]

[13]. Ensign LM, Cone R, Hanes J, Nanoparticle-based drug delivery to the vagina: a review, J Control Release, 190 (2014) 500–514. [PubMed: 24830303]

[14]. Baelo A, Levato R, Julian E, Crespo A, Astola J, Gavalda J, Engel E, Mateos-Timoneda MA, Torrents E, Disassembling bacterial extracellular matrix with DNase-coated nanoparticles to enhance antibiotic delivery in biofilm infections, J Control Release, 209 (2015) 150–158. [PubMed: 25913364]

[15]. Steinbach JM, Protein and oligonucleotide delivery systems for vaginal microbicides against viral STIs, Cell Mol Life Sci, 72 (2015) 469–503. [PubMed: 25323132]

[16]. Chee WJY, Chew SY, Than LTL, Vaginal microbiota and the potential of Lactobacillus derivatives in maintaining vaginal health, Microb Cell Fact, 19 (2020) 203. [PubMed: 33160356]

[17]. Sung YK, Kim SW, Recent advances in polymeric drug delivery systems, Biomaterials Research, 24 (2020).

[18]. Rafiei F, Tabesh H, Farzad S, Farzaneh F, Rezaei M, Hosseinzade F, Mottaghy K, Development of Hormonal Intravaginal Rings: Technology and Challenges, Geburtshilfe Frauenheilkd, 81 (2021) 789–806. [PubMed: 34276064]

[19]. Tighe BJ, A decade of silicone hydrogel development: surface properties, mechanical properties, and ocular compatibility, Eye Contact Lens, 39 (2013) 4–12. [PubMed: 23292050]

[20]. Naumovski B, Kapushevska B, Dimensional Stability and Acuracy of Silicone - Based Impression Materials Using Different Impression Techniques - A Literature Review, Pril (Makedon Akad Nauk Umet Odd Med Nauki), 38 (2017) 131–138. [PubMed: 28991761]

[21]. Schubert C, van Langeveld MC, Donoso LA, Innovations in 3D printing: a 3D overview from optics to organs, Br J Ophthalmol, 98 (2014) 159–161. [PubMed: 24288392]

[22]. Vaz VM, Kumar L, 3D Printing as a Promising Tool in Personalized Medicine, AAPS PharmSciTech, 22 (2021).

[23]. Karavasili C, Eleftheriadis GK, Gioumouxouzis C, Andriotis EG, Fatouros DG, Mucosal drug delivery and 3D printing technologies: A focus on special patient populations, Adv Drug Deliv Rev, 176 (2021) 113858. [PubMed: 34237405]

[24]. Fu J, Yu X, Jin Y, 3D printing of vaginal rings with personalized shapes for controlled release of progesterone, Int J Pharm, 539 (2018) 75–82. [PubMed: 29366944]

[25]. Tiboni M, Campana R, Frangipani E, Casettari L, 3D printed clotrimazole intravaginal ring for the treatment of recurrent vaginal candidiasis, Int J Pharm, 596 (2021) 120290. [PubMed: 33524521]

[26]. Elkasabgy NA, Mahmoud AA, Maged A, 3D printing: An appealing route for customized drug delivery systems, Int J Pharm, 588 (2020) 119732. [PubMed: 32768528]

[27]. Janusziewicz R, Mecham SJ, Olson KR, Benhabbour SR, Design and Characterization of a Novel Series of Geometrically Complex Intravaginal Rings with Digital Light Synthesis, Adv Mater Technol, 5 (2020).

[28]. Sethi R, Cunha A, Mellis K, Siauw T, Diederich C, Pouliot J, Hsu IC, Clinical applications of custom-made vaginal cylinders constructed using three-dimensional printing technology, J Contemp Brachytherapy, 8 (2016) 208–214. [PubMed: 27504130]

[29]. Hou C, Zheng J, Li Z, Qi X, Tian Y, Zhang M, Zhang J, Huang X, Printing 3D vagina tissue analogues with vagina decellularized extracellular matrix bioink, Int J Biol Macromol, 180 (2021) 177–186. [PubMed: 33737175]

[30]. Suriboot J, Marmo AC, Ngo BKD, Nigam A, Ortiz-Acosta D, Tai BL, Grunlan MA, Amphiphilic, thixotropic additives for extrusion-based 3D printing of silica-reinforced silicone, Soft Matter, 17 (2021) 4133–4142. [PubMed: 33735370]

[31]. Rodriguez N, Ruelas S, Forien J-B, Dudukovic N, Deotte J, Rodriguez J, Moran B, Lewicki JP, Duoss EB, Oakdale JS, 3D Printing of High Viscosity Reinforced Silicone Elastomers, Polymers, 13 (2021) 2239. [PubMed: 34300996]

[32]. Razavi M, Primavera R, Vykunta A, Thakor AS, Silicone-based bioscaffolds for cellular therapies, Mater Sci Eng C Mater Biol Appl, 119 (2021) 111615. [PubMed: 33321658]

[33]. Eder S, et al. , Toward a new generation of vaginal pessaries via 3D-printing: Concomitant mechanical support and drug delivery, European Journal of Pharmaceutics and Biopharmaceutics, 174 (2022) 77. [PubMed: 35390451]

[34]. Spoerk M, et al. , Personalised urethra pessaries prepared by material extrusion-based additive manufacturing, International Journal of Pharmaceutics, 608 (2021) 121112. [PubMed: 34547391]

[35]. Barnhart KT, Izquierdo A, Pretorius ES, Shera DM, Shabbout M, Shaunik A, Baseline dimensions of the human vagina, Human Reproduction, 21 (2006) 1618–1622. [PubMed: 16478763]

[36]. Tappa K, et al. , Medication eluting devices for the field of OBGYN (MEDOBGYN): 3D printed biodegradable hormone eluting constructs, a proof of concept study, PLoS ONE, 12 (2017) 0182929.

[37]. Koutsamanis I, Paudel A, Alva Zúñiga CP, Wiltschko L, Spoerk M, Novel polyester-based thermoplastic elastomers for 3D-printed long-acting drug delivery applications, J Control Release, 335 (2021) 290–305. [PubMed: 34044092]

[38]. Domínguez-Robles J, Mancinelli C, Mancuso E, García-Romero I, Gilmore BF, Casettari L, Larrañeta E, Lamprou DA, 3D Printing of Drug-Loaded Thermoplastic Polyurethane Meshes: A Potential Material for Soft Tissue Reinforcement in Vaginal Surgery, Pharmaceutics, 12 (2020).

[39]. Arany P, Papp I, Zichar M, Regdon G, Béres M, Szalóki M, Kovács R, Fehér P, Ujhelyi Z, Vecsernyés M, Bácskay I, Manufacturing and Examination of Vaginal Drug Delivery System by FDM 3D Printing, Pharmaceutics, 13 (2021) 1714. [PubMed: 34684007]

[40]. Genina N, et al. , Ethylene vinyl acetate (EVA) as a new drug carrier for 3D printed medical drug delivery devices, European Journal of Pharmaceutical Sciences, 90 (2016) 53. [PubMed: 26545484]

[41]. Gómez-Blanco JC, Mancha-Sánchez E, Marcos AC, Matamoros M, Díaz-Parralejo A, Pagador JB, Bioink Temperature Influence on Shear Stress, Pressure and Velocity Using Computational Simulation, Processes, 8 (2020) 865.

[42]. Cooke ME, Rosenzweig DH, The rheology of direct and suspended extrusion bioprinting, APL Bioengineering, 5 (2021) 011502. [PubMed: 33564740]

[43]. Jamroz W, Szafraniec J, Kurek M, Jachowicz R, 3D Printing in Pharmaceutical and Medical Applications - Recent Achievements and Challenges, Pharm Res, 35 (2018) 176. [PubMed: 29998405]

[44]. Ring TP, Langer SC, Design, Experimental and Numerical Characterization of 3D-Printed Porous Absorbers, Materials, 12 (2019) 3397. [PubMed: 31627354]

[45]. Siepmann J, Siepmann F, Mathematical modeling of drug delivery, International Journal of Pharmaceutics, 364 (2008) 328. [PubMed: 18822362]

[46]. Karakurt I, Aydoğdu A, Çıkrıkcı S, Orozco J, Lin L, Stereolithography (SLA) 3D printing of ascorbic acid loaded hydrogels: A controlled release study, Int J Pharm, 584 (2020) 119428. [PubMed: 32445906]

[47]. Wang P, Berry DB, Song Z, Kiratitanaporn W, Schimelman J, Moran A, He F, Xi B, Cai S, Chen S, 3D Printing of a Biocompatible Double Network Elastomer with Digital Control of Mechanical Properties, Advanced Functional Materials, 30 (2020) 1910391. [PubMed: 33071708]

[48]. Luo Y, Le Fer G, Dean D, Becker ML, 3D Printing of Poly(propylene fumarate) Oligomers: Evaluation of Resin Viscosity, Printing Characteristics and Mechanical Properties, Biomacromolecules, 20 (2019) 1699–1708. [PubMed: 30807696]

[49]. Angelis MD, Gobbetti M, Environmental stress responses inLactobacillus: A review, Proteomics, 4 (2004) 106. [PubMed: 14730676]

[50]. Corcoran B, et al. , Life Under Stress: The Probiotic Stress Response and How it may be Manipulated, Current Pharmaceutical Design, 14 (2008) 1382. [PubMed: 18537661]

[51]. Amund OD, Exploring the relationship between exposure to technological and gastrointestinal stress and probiotic functional properties of lactobacilli and bifidobacteria, Canadian Journal of Microbiology, 62 (2016) 715–725. [PubMed: 27461506]

[52]. Baral KC, Bajracharya R, Lee SH, Han H-K, Advancements in the Pharmaceutical Applications of Probiotics: Dosage Forms and Formulation Technology, International Journal of Nanomedicine, Volume 16 (2021) 7535–7556. [PubMed: 34795482]

[53]. Gurram S, Jha DK, Shah DS, Kshirsagar MM, Amin PD, Insights on the Critical Parameters Affecting the Probiotic Viability During Stabilization Process and Formulation Development, AAPS PharmSciTech, 22 (2021).

[54]. Estermann SJ, Pahr DH, Reisinger A, Quantifying tactile properties of liver tissue, silicone elastomers, and a 3D printed polymer for manufacturing realistic organ models, Journal of the Mechanical Behavior of Biomedical Materials, 104 (2020) 103630. [PubMed: 32174390]

[55]. Zaveri T, Primrose RJ, Surapaneni L, Ziegler GR, Hayes JE, Firmness Perception Influences Women's Preferences for Vaginal Suppositories, Pharmaceutics, 6 (2014) 512–529. [PubMed: 25211123]

[56]. Asnaashari S, Khoei NS, Zarrintan MH, Adibkia K, Javadzadeh Y, Preparation and evaluation of novel metronidazole sustained release and floating matrix tablets, Pharm Dev Technol, 16 (2011) 400–407. [PubMed: 20429828]

[57]. Owen DH, Katz DF, A vaginal fluid simulant, Contraception, 59 (1999) 91–95. [PubMed: 10361623]

[58]. Tietz K, Klein S, Simulated Genital Tract Fluids and Their Applicability in Drug Release/ Dissolution Testing of Vaginal Dosage Forms, Dissolution Technologies, 25 (2018) 40–51.

[59]. Bashi YHD, et al. , Silicone elastomer formulations for improved performance of a multipurpose vaginal ring releasing dapivirine and levonorgestrel, International Journal of Pharmaceutics: X, 3 (2021) 100091.

[60]. Lukin RY, Kuchkaev AM, Sukhov AV, Bekmukhamedov GE, Yakhvarov DG, Platinum-Catalyzed Hydrosilylation in Polymer Chemistry, Polymers (Basel), 12 (2020).

[61]. Inglis DW, A method for reducing pressure-induced deformation in silicone microfluidics, Biomicrofluidics, 4 (2010) 026504. [PubMed: 20697573]

[62]. Bakke AJ, Zaveri T, Higgins MJ, Ziegler GR, Hayes JE, Design aspects of vaginal applicators that influence acceptance among target users, Scientific Reports, 11 (2021).

[63]. Liu X, Champagne CP, Lee BH, Boye JI, Casgrain M, Thermostability of Probiotics and Their alpha -Galactosidases and the Potential for Bean Products, Biotechnol Res Int, 2014 (2014) 472723. [PubMed: 24744923]

[64]. Hua Y, Lyu C, Liu C, Wang H, Hu S, Zhao W, Mei J, Huang J, Mei L, Improving the Thermostability of Glutamate Decarboxylase from Lactobacillus brevis by Consensus Mutagenesis, Appl Biochem Biotechnol, 191 (2020) 1456–1469. [PubMed: 32124175]

[65]. Slattery L, O'Callaghan J, Fitzgerald GF, Beresford T, Ross RP, Invited review: Lactobacillus helveticus—A thermophilic dairy starter related to gut bacteria, Journal of Dairy Science, 93 (2010) 4435–4454. [PubMed: 20854978]

[66]. Anjum N, Maqsood S, Masud T, Ahmad A, Sohail A, Momin A, Lactobacillus acidophilus: characterization of the species and application in food production, Crit Rev Food Sci Nutr, 54 (2014) 1241–1251. [PubMed: 24499153]

[67]. Simonenko ES, Begunova AV, [Development of fermented milk product based on mare milk and lactic microorganisms association], Vopr Pitan, 90 (2021) 115–125. [PubMed: 34719149]

[68]. Verstraete G, et al. , Thermoplastic polyurethane-based intravaginal rings for prophylaxis and treatment of (recurrent) bacterial vaginosis, International Journal of Pharmaceutics, 529 (2017) 218. [PubMed: 28663088]

[69]. De Souza NAB, Souza FSD, Basílio ID Jr, Medeiros ACD, Oliveira EJ, Santos AFO, Macwdo RO, Macędo RO, Journal of Thermal Analysis and Calorimetry, 72 (2003) 535–538.

[70]. Li S, Culkin A, Jones DS, Andrews GP, Development of Polycaprolactone-Based metronidazole matrices for intravaginal extended drug delivery using a mechanochemically prepared therapeutic deep eutectic system, Int J Pharm, 593 (2021) 120071. [PubMed: 33246048]

[71]. Ajjarapu S, Rangappa S, Shankar VK, Shettar A, Kumar HNS, Kulkarni VI, Repka MA, Murthy SN, A Rapid Tool to Optimize Process Variables for Continuous Manufacturing of Metronidazole Ointment Using Melt Extrusion Technique, AAPS PharmSciTech, 21 (2020).

[72]. Petrina MAB, Cosentino LA, Rabe LK, Hillier SL, Susceptibility of bacterial vaginosis (BV)-associated bacteria to secnidazole compared to metronidazole, tinidazole and clindamycin, Anaerobe, 47 (2017) 115–119. [PubMed: 28522362]

[73]. Johnson TJ, Gupta KM, Fabian J, Albright TH, Kiser PF, Segmented polyurethane intravaginal rings for the sustained combined delivery of antiretroviral agents dapivirine and tenofovir, European Journal of Pharmaceutical Sciences, 39 (2010) 203–212. [PubMed: 19958831]

[74]. Clark JT, Johnson TJ, Clark MR, Nebeker JS, Fabian J, Tuitupou AL, Ponnapalli S, Smith EM, Friend DR, Kiser PF, Quantitative evaluation of a hydrophilic matrix intravaginal ring for the sustained delivery of tenofovir, J Control Release, 163 (2012) 240–248. [PubMed: 22981701]

[75]. Dash S, Murthy PN, Nath L, Chowdhury P, Kinetic modeling on drug release from controlled drug delivery systems, Acta Pol Pharm, 67 (2010) 217–223. [PubMed: 20524422]

[76]. Higuchi T, MECHANISM OF SUSTAINED-ACTION MEDICATION. THEORETICAL ANALYSIS OF RATE OF RELEASE OF SOLID DRUGS DISPERSED IN SOLID MATRICES, J Pharm Sci, 52 (1963) 1145–1149. [PubMed: 14088963]

[77]. Costa P, Sousa Lobo JM, Modeling and comparison of dissolution profiles, Eur J Pharm Sci, 13 (2001) 123–133.

[78]. Peppas NA, Sahlin JJ, A simple equation for the description of solute release. III. Coupling of diffusion and relaxation, International Journal of Pharmaceutics, 57 (1989) 169.

[79]. Latha S, Selvamani P, Kumar CS, Sharavanan P, Suganya G, Beniwal V, Rao PR, Formulation development and evaluation of metronidazole magnetic nanosuspension as a magnetic-targeted and polymeric-controlled drug delivery system, Journal of Magnetism and Magnetic Materials, 321 (2009) 1580–1585.

[80]. Ozyazici M, Gökçe EH, Ertan G, Release and diffusional modeling of metronidazole lipid matrices, Eur J Pharm Biopharm, 63 (2006) 331–339. [PubMed: 16621486]

[81]. Wróblewska M, Szymańska E, Szekalska M, Winnicka K, Different Types of Gel Carriers as Metronidazole Delivery Systems to the Oral Mucosa, Polymers (Basel), 12 (2020).

[82]. Forbes CJ, Lowry D, Geer L, Veazey RS, Shattock RJ, Klasse PJ, Mitchnick M, Goldman L, Doyle LA, Muldoon BC, Woolfson AD, Moore JP, Malcolm RK, Non-aqueous silicone

elastomer gels as a vaginal microbicide delivery system for the HIV-1 entry inhibitor maraviroc, J Control Release, 156 (2011) 161–169. [PubMed: 21864598]

[83]. Zhao P, Tong Y, Ma N, Han B, Dong X, Qi M, Molecular Dynamics Simulations and Experimental Studies of the Microstructure and Mechanical Properties of a Silicone Oil/Functionalized Ionic Liquid-Based Magnetorheological Fluid, ACS Applied Materials & Interfaces, 14 (2022) 10987–10997. [PubMed: 35175022]

[84]. Fanse S, et al. , Effect of crosslinking on the physicochemical properties of polydimethylsiloxane-based levonorgestrel intrauterine systems, International Journal of Pharmaceutics, 609 (2021) 121192. [PubMed: 34666142]

[85]. Wu Y, Liu J, Jiao X, Cheng F, Lai G, Yang X, UV-Cured Transparent Flexible Silicone Materials with High Tensile Strength, ACS Omega, 5 (2020) 6199–6206. [PubMed: 32226905]

[86]. Jiao X, Liu J, Jin J, Cheng F, Fan Y, Zhang L, Lai G, Hua X, Yang X, UV-Cured Transparent Silicone Materials with High Tensile Strength Prepared from Hyperbranched Silicon-Containing Polymers and Polyurethane-Acrylates, ACS Omega, 6 (2021) 2890–2898. [PubMed: 33553907]

[87]. Fanse S, et al. , Impact of polymer crosslinking on release mechanisms from long-acting levonorgestrel intrauterine systems, International Journal of Pharmaceutics, 612 (2022) 121383. [PubMed: 34919997]

[88]. Lowder JL, Debes KM, Moon DK, Howden N, Abramowitch SD, Moalli PA, Biomechanical adaptations of the rat vagina and supportive tissues in pregnancy to accommodate delivery, Obstet Gynecol, 109 (2007) 136–143. [PubMed: 17197599]

[89]. Robison KM, Conway CK, Desrosiers L, Knoepp LR, Miller KS, Biaxial Mechanical Assessment of the Murine Vaginal Wall Using Extension–Inflation Testing, Journal of Biomechanical Engineering, 139 (2017).

[90]. Clark GL, Pokutta-Paskaleva AP, Lawrence DJ, Lindsey SH, Desrosiers L, Knoepp LR, Bayer CL, Gleason RL, Miller KS, Smooth muscle regional contribution to vaginal wall function, Interface Focus, 9 (2019) 20190025. [PubMed: 31263538]

[91]. Constantinou CE, Omata S, Direction sensitive sensor probe for the evaluation of voluntary and reflex pelvic floor contractions, Neurourol Urodyn, 26 (2007) 386–391. [PubMed: 17301962]

[92]. Spoerk M, Arbeiter F, Koutsamanis I, Cajner H, Katschnig M, Eder S, Personalised urethra pessaries prepared by material extrusion-based additive manufacturing, Int J Pharm, 608 (2021) 121112. [PubMed: 34547391]

[93]. Eberhart R, Chuong CJ, Zimmern P, Exploring biomechanical methods to study the human vaginal wall, Neurourol Urodyn, 36 (2017) 499–506. [PubMed: 26828789]

[94]. Kim JH, Urogynecology and Reconstructive Pelvic Surgery. 4th ed, Int Neurourol J, 19 (2015) 51. [PubMed: 25833482]

[95]. Snorradóttir BS, Jónsdóttir F, Sigurdsson ST, Thorsteinsson F, Másson M, Numerical modelling and experimental investigation of drug release from layered silicone matrix systems, Eur J Pharm Sci, 49 (2013) 671–678. [PubMed: 23684932]

[96]. Krenzlin S, Vincent C, Munzke L, Gnansia D, Siepmann J, Siepmann F, Predictability of drug release from cochlear implants, J Control Release, 159 (2012) 60–68. [PubMed: 22233971]

[97]. Javadzadeh Y, Hamedeyazdan S, Adibkia K, Kiafar F, Zarrintan MH, Barzegar-Jalali M, Evaluation of drug release kinetics and physico-chemical characteristics of metronidazole floating beads based on calcium silicate and gas-forming agents, Pharm Dev Technol, 15 (2010) 329–338. [PubMed: 19694496]

[98]. Calija B, Cekić N, Savić S, Krajišnik D, Daniels R, Milić J, An investigation of formulation factors affecting feasibility of alginate-chitosan microparticles for oral delivery of naproxen, Arch Pharm Res, 34 (2011) 919–929. [PubMed: 21725813]

[99]. Sabbatini S, Monari C, Ballet N, Decherf AC, Bozza S, Camilloni B, Perito S, Vecchiarelli A, Anti-Biofilm Properties of Saccharomyces cerevisiae CNCM I-3856 and Lacticaseibacillus rhamnosus ATCC 53103 Probiotics against G. vaginalis, Microorganisms, 8 (2020).

[100]. Cirri M, Maestrelli F, Scuota S, Bazzucchi V, Mura P, Development and microbiological evaluation of chitosan and chitosan-alginate microspheres for vaginal administration of metronidazole, Int J Pharm, 598 (2021) 120375. [PubMed: 33581271]

[101]. Johansson AK, Johansson A, Stan V, Ohlson CG, Silicone sealers, acetic acid vapours and dental erosion: a work-related risk?, Swed Dent J, 29 (2005) 61–69. [PubMed: 16035349]

[102]. Fuchs W, Brockmeyer NH, Sexually transmitted infections JDDG: Journal der Deutschen Dermatologischen Gesellschaft, 12 (2014) 451–464. [PubMed: 24889293]

[103]. Cook MT, Brown MB, Polymeric gels for intravaginal drug delivery, Journal of Controlled Release, 270 (2018) 145–157. [PubMed: 29223536]

[104]. Faught BM, Reyes S, Characterization and Treatment of Recurrent Bacterial Vaginosis, J Womens Health (Larchmt), 28 (2019) 1218–1226. [PubMed: 31403349]

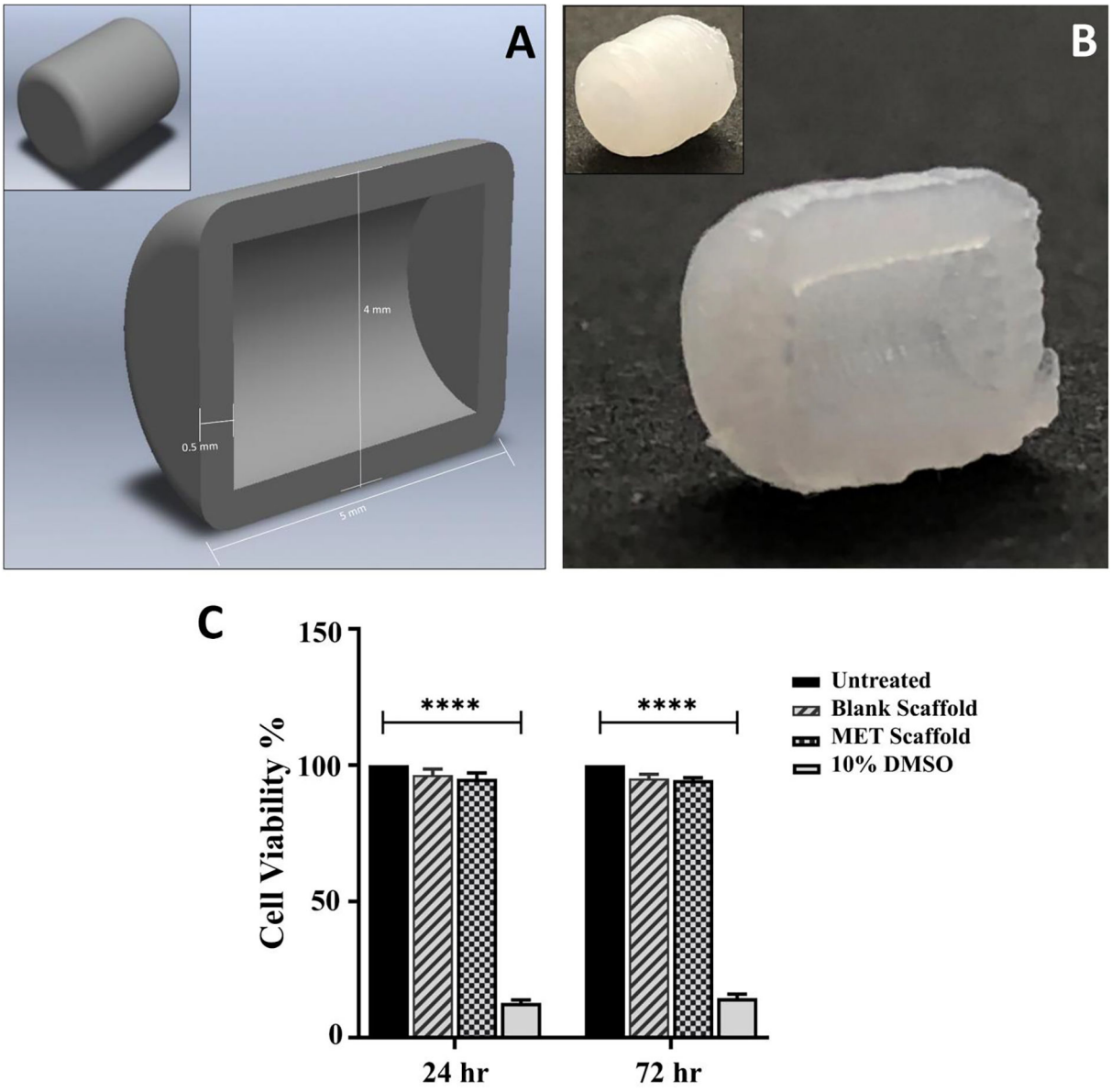

Figure 1.

3D-printed scaffold design. (A) CAD representative image of cross-sectional and isometric view; (B) Actual image of cross-sectional and isometric view; (C) VK2 cell viability after exposure to the scaffolds.

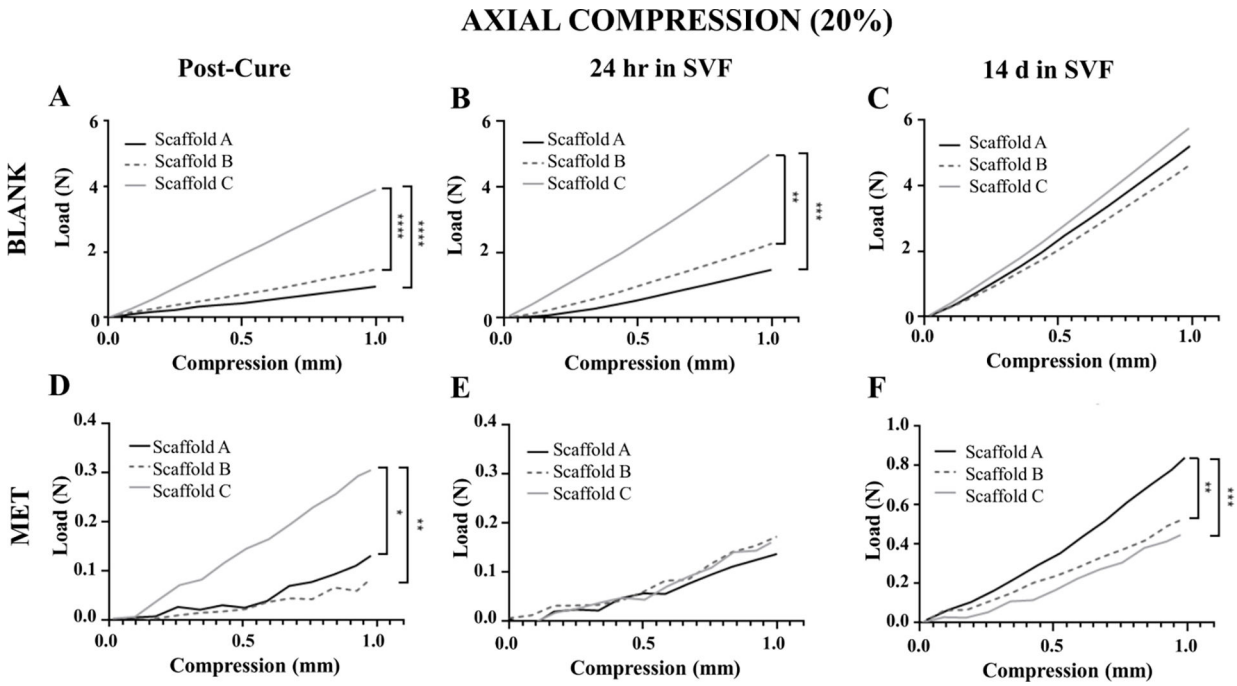

Figure 2.

Blank silicone and metronidazole-containing scaffolds were evaluated under 20% axial compression as a function of curing condition (Scaffolds A, B, and C), immediately post-cure and after 24 hr and 14 d in SVF. Load is shown as a function of axial compression of blank scaffolds (Panels A-C) and metronidazole-containing scaffolds (Panels D-F). Mechanical testing was performed using five replicates per curing condition. Statistical significance between experimental groups, as calculated by one-way ANOVA, is represented by *$p \leq 0.05$, **$p \leq 0.01$, ***$p \leq 0.001$, ****$p \leq 0.0001$. Note y-axes scale differences between the various conditions.

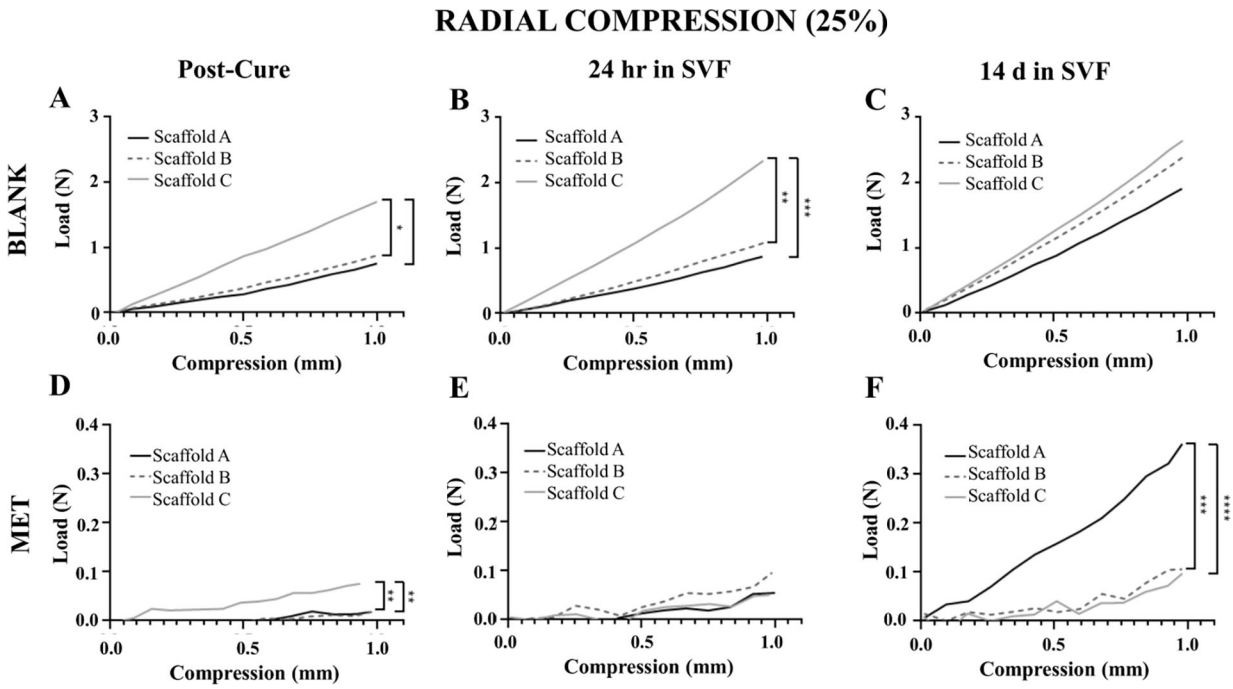

Figure 3.

Blank silicone and metronidazole-containing scaffolds were evaluated under 25% radial compression as a function of curing condition (Scaffolds A, B, and C), immediately post-cure and after 24 hr and 14 d in SVF. Load is shown as a function of radial compression of blank scaffolds (Panels A-C) and metronidazole-containing scaffolds (Panels D-F). Mechanical testing was performed using five replicates per curing condition. Statistical significance between experimental groups, as calculated by one-way ANOVA, is represented by *$p \leq 0.05$, **$p \leq 0.01$, ***$p \leq 0.001$, ****$p \leq 0.0001$. Note y-axes scale differences between the various conditions.

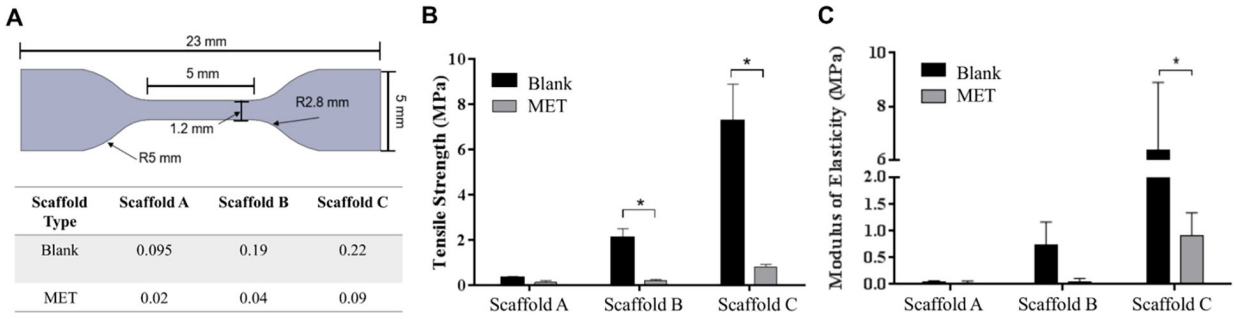

Scaffold Type	Scaffold A	Scaffold B	Scaffold C
Blank	0.095	0.19	0.22
MET	0.02	0.04	0.09

Figure 4.

(A) Representative of the scaled die cut C dog bone specimen for tensile testing in accordance with ASTM D412 standards, and table of strain values for blank and metronidazole-containing scaffolds. (B) Tensile strength and (C) elastic modulus of blank and metronidazole-containing scaffolds tensile tested to rupture. Tensile testing was performed using three replicates per curing condition. Statistical significance between experimental groups, as calculated by paired t-test, is represented by *$p \leq 0.05$.

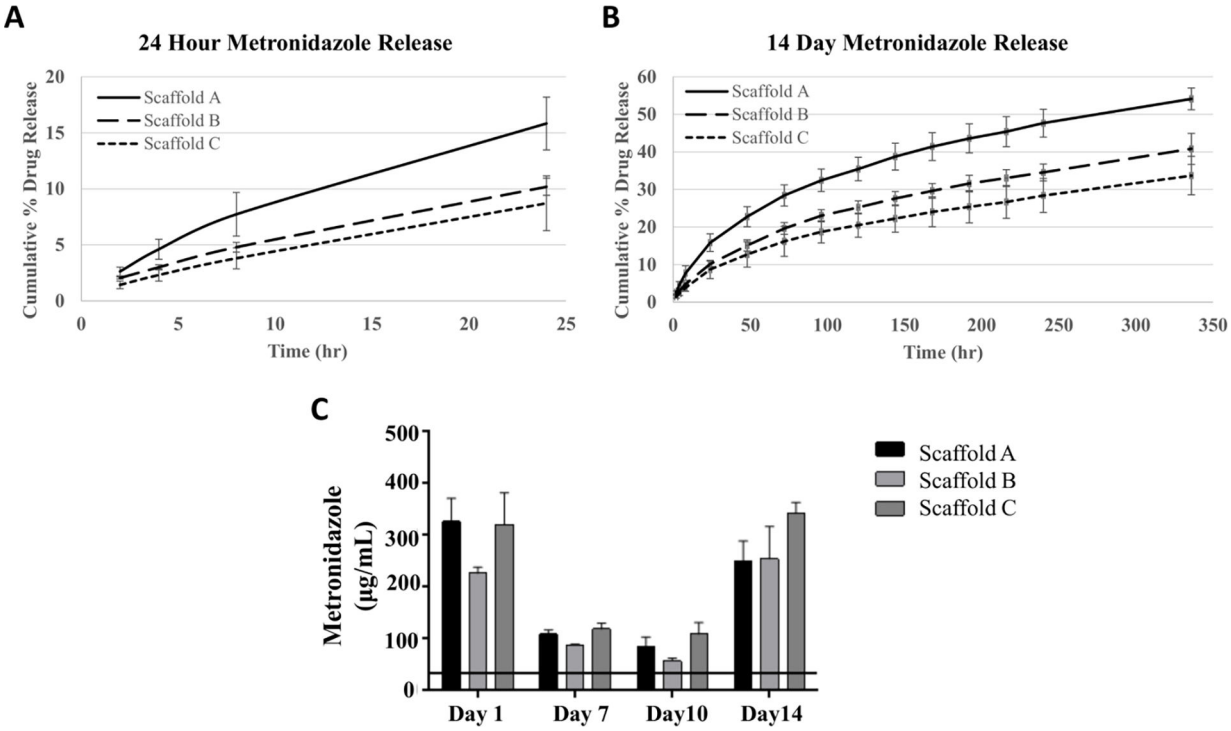

Figure 5.

Metronidazole release in SVF from 3D printed scaffolds. (A) Short-term release over 24 hr. (B) Long-term release over 14 d. For both short-term and long-term release, statistical significance was observed between Scaffolds A and B and between Scaffolds A and C ($p \leq 0.05$), (C) Metronidazole amount released (μg/ 1 ml SVF) from 1 to 14 d. For all scaffolds, amount was >32 μg/ml, (horizontal line), which represents bactericidal concentration of metronidazole against *Gardnerella vaginalis* biofilm viability at concentration of 10^8 CFU/ml [99]. Error bars represent standard deviation (n=3).

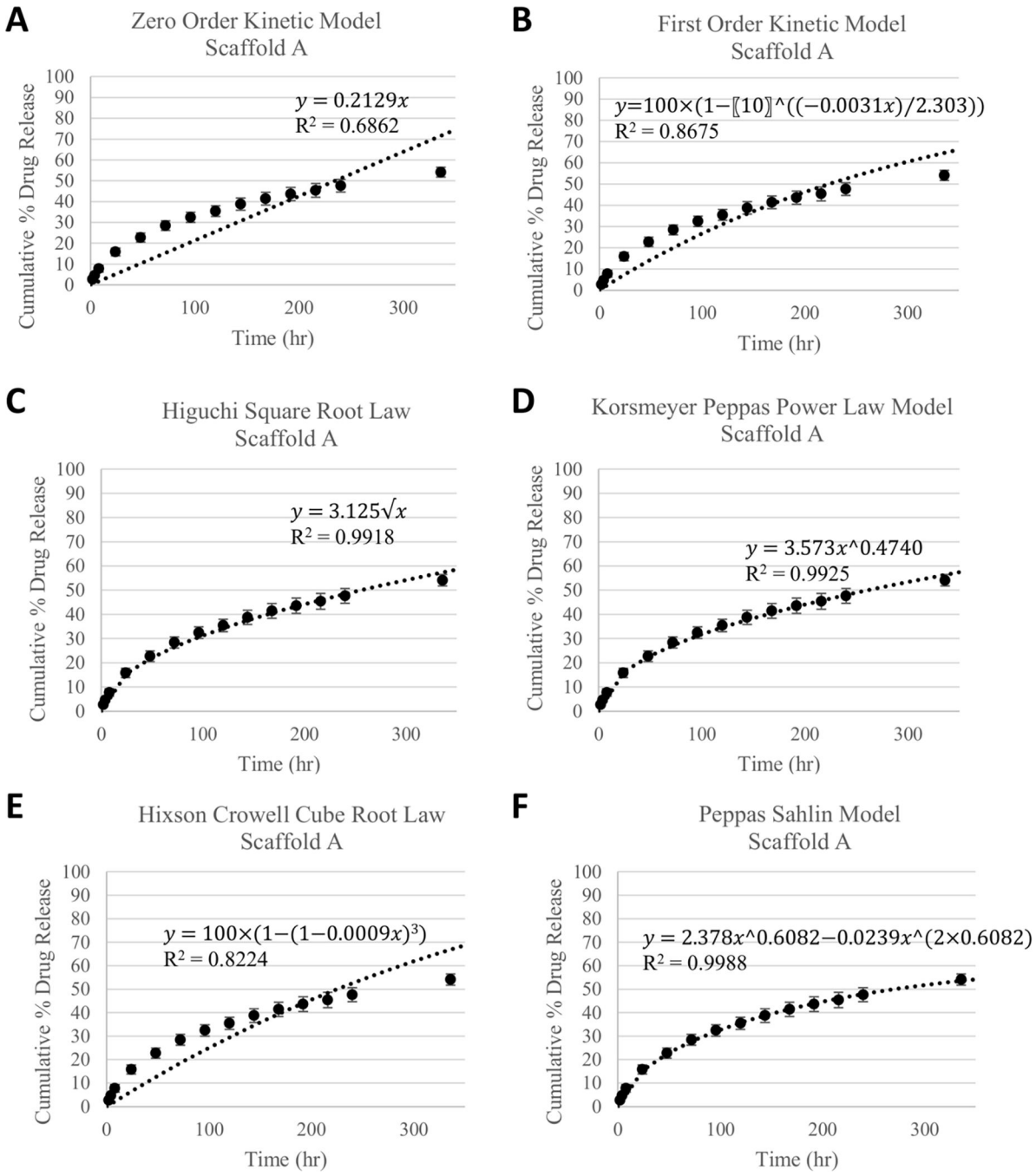

Figure 6.

Metronidazole release from Scaffold A fitted to A) Zero order kinetic, B) First order kinetic, C) Higuchi, D) Korsmeyer-Peppas, E) Hixson Crowell, and F) Peppas-Sahlin models. The equation of best fit line and R^2 values, representing the adequacy of the fit, are shown on each plot.

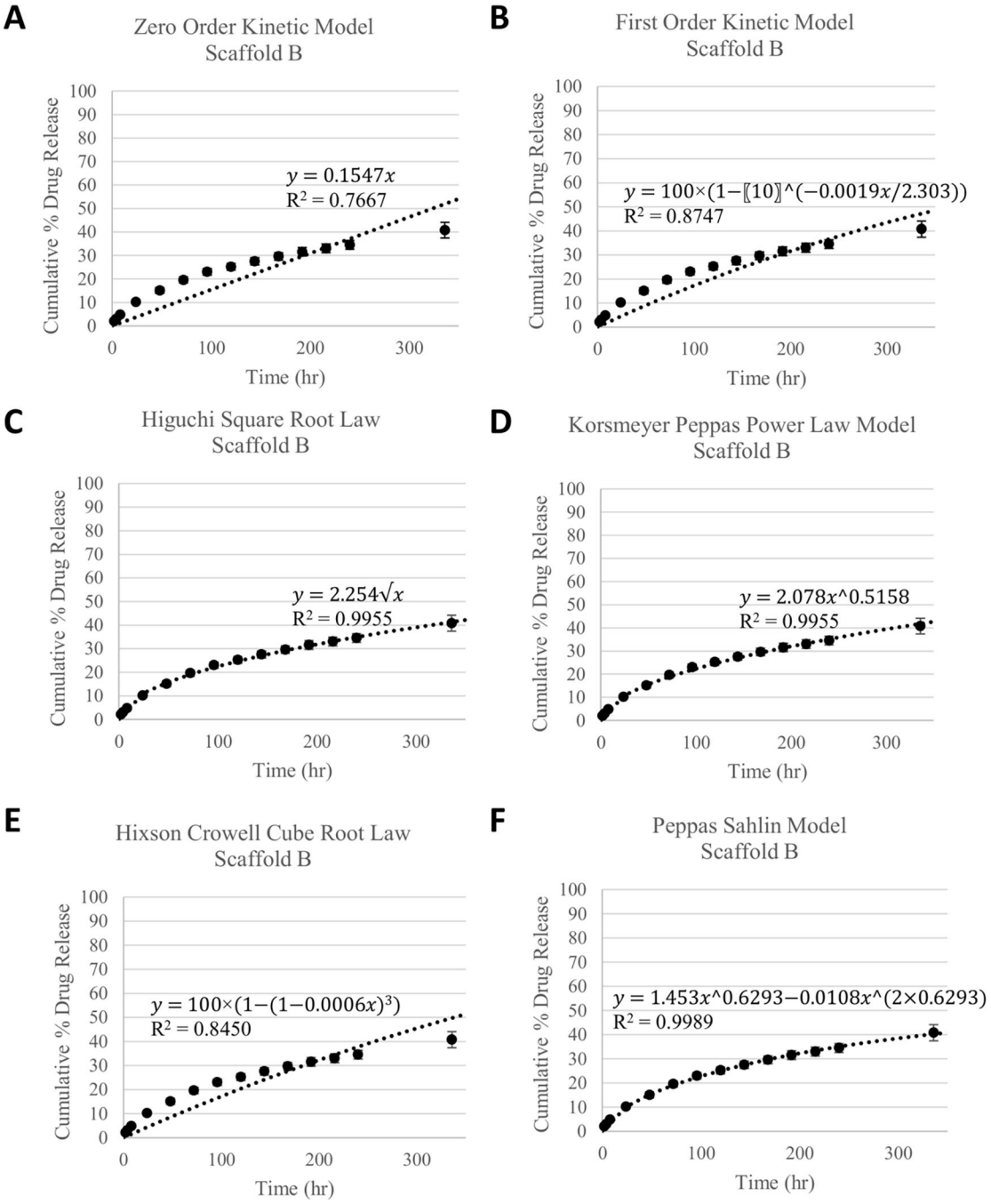

Figure 7.

Metronidazole release from Scaffold B fitted to A) Zero order kinetic, B) First order kinetic, C) Higuchi, D) Korsmeyer-Peppas, E) Hixson Crowell, and F) Peppas-Sahlin models. The equation of best fit line and R^2 values, representing the adequacy of the fit, are shown on each plot.

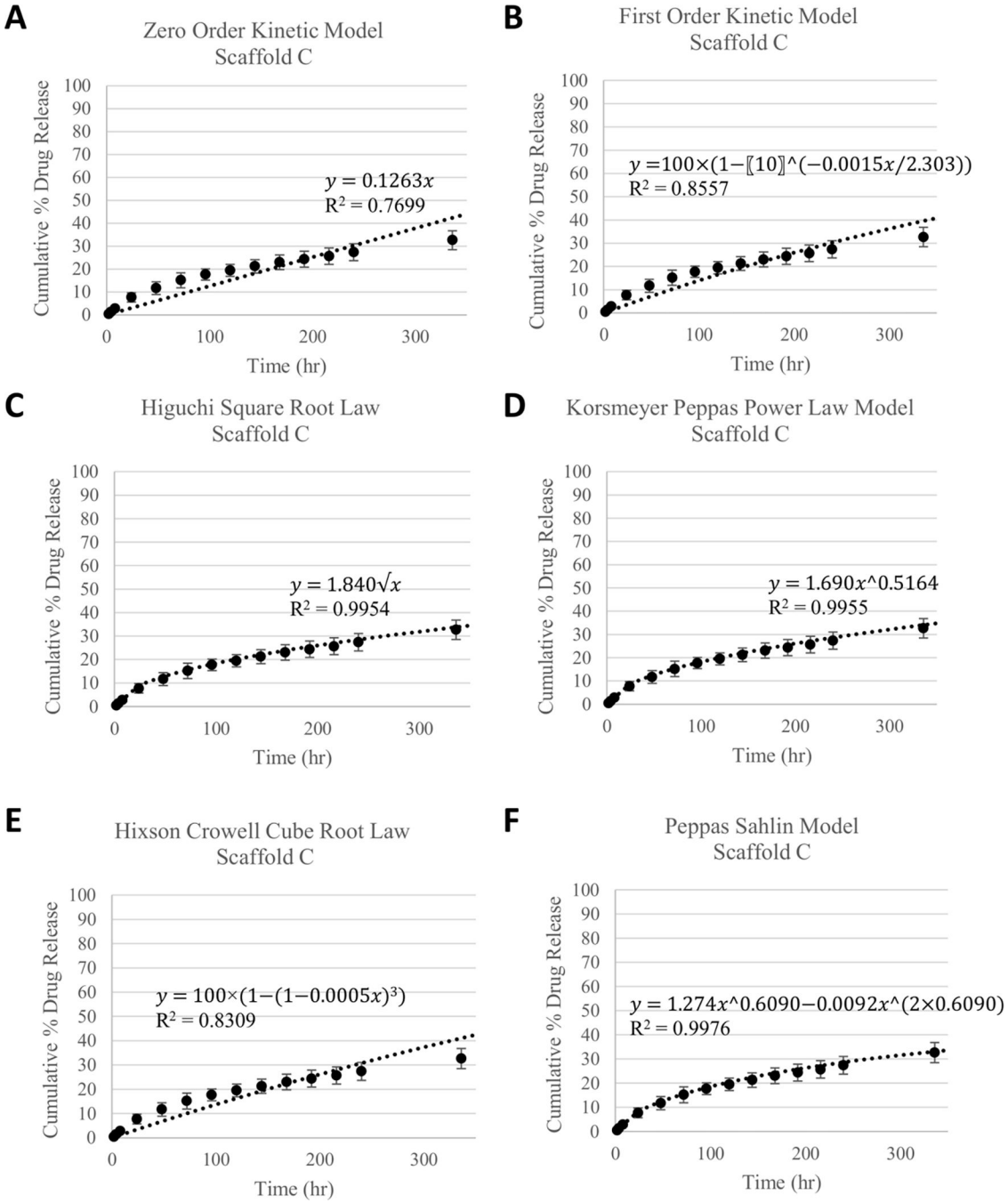

Figure 8.

Metronidazole release from Scaffold C fitted to A) Zero Order kinetic, B) First Order kinetic, C) Higuchi, D) Korsmeyer-Peppas, E) Hixson Crowell, and F) Peppas-Sahlin models. The equation of best fit line and R^2 values, representing the adequacy of the fit, are shown on each plot.

Table 1.

Correlation values and rate constants of each kinetic model for Scaffolds A, B, and C.

Model	Scaffold		
	A	B	C
Zero Order Kinetic Model	k = 0.2129 R^2 = 0.6862	k = 0.1547 R^2 = 0.7667	k = 0.1263 R^2 = 0.7699
First Order Kinetic Model	k = 0.0023 R^2 = 0.9438	k = 0.0015 R^2 = 0.9494	k = 0.0012 R^2 = 0.9442
Higuchi Square Root Model	k = 3.125 R^2 = 0.9918	k = 2.254 R^2 = 0.9955	k = 1.840 R^2 = 0.9954
Korsmeyer-Peppas Model	k = 3.573 n = 0.4740 R^2 = 0.9931	k = 2.078 n = 0.5158 R^2 = 0.9959	k = 1.690 n = 0.5164 R^2 = 0.9958
Peppas-Sahlin Model	k_d = 2.378 k_r = −0.2390 m = 0.6082 R^2 = 0.9990	k_d = 1.453 k_r = −0.0107 m = 0.6293 R^2 = 0.9990	k_d = 1.274 k_r = −0.0091 m = 0.6090 R^2 = 0.9980
Hixson-Crowell Model	k = 0.0009 R^2 = 0.8224	k = 0.0006 R^2 = 0.8450	k = 0.0005 R^2 = 0.8304